PHYSICAL REVIEW E **78**, 050801(R) (2008)

Microvoid formation and strain hardening in highly cross-linked polymer networks

Debashish Mukherji* and Cameron F. Abrams
Department of Chemical and Biological Engineering, Drexel University, Philadelphia, Pennsylvania 19104, USA
(Received 26 June 2008; revised manuscript received 8 October 2008; published 4 November 2008)

Using molecular dynamics simulations of a generic model, we observe strain hardening in highly cross-linked polymer glasses under tensile deformation. We show that formation of microvoids, without bond breaking, constitutes the microscopic origins of strain hardening. A well-defined functional form is observed for the void size distribution that is consistent with voids in dense equilibrium Lennard-Jones particle packings, independent of strain. Microvoid-based strain hardening is not observed in a separate model with tetrahedral bond angle constraints, indicating that flexible cross-linkers are the key factor in the development of strain hardening behavior.

DOI: 10.1103/PhysRevE.78.050801 PACS number(s): 61.41.+e, 83.10.Rs, 87.15.La

Understanding the links between molecular structure and the mechanical properties of polymeric materials is theoretically challenging, but has enormous technological importance. Interest in this field is motivated by the possible implications in designing better adhesives and composite materials [1,2]. Traditionally much effort has been devoted to understand the molecular origins of the response of materials comprised of linear and branched polymers to deformation [3–5]. More recent interest has been directed toward understanding the underlying phenomena that govern the mechanical properties of highly cross-linked polymer networks [6–8].

Highly cross-linked polymers (HCPs) are three-dimensional networks of covalently connected monomers, i.e., each multifunctional monomer can form bonds with several nearest neighbors. Examples are epoxy and vinyl-ester thermosets, used as both high-strength adhesives and as composite matrices. These materials exhibit a wide range of exotic and unpredictable features, such as self-healing [7,9–11] and pressure-sensitive adhesion [12]. However, despite advances in the development of HCPs with improved performance, theoretical approaches in this field are relatively limited. More specifically, the complexity of the molecular-level structure of HCPs and its direct connection to physical properties are generally poorly understood. Therefore simulations have become a popular method [6,8,13,14] to ascertain what determines the mechanical properties of HCPs.

One particular property of HCPs that limits their usefulness is their lack of ductility. For example, fully cured epoxies can be strong (i.e., about 2 GPa tensile strength) but brittle (failing at about 1% tensile strain). Therefore it is worthwhile to investigate how one might generate a HCP network that exhibits ductility. While current understanding is solely attributed to the effect of cross-linker density on ductility of a HCP network [15], we suggest a way to control ductility by keeping this density constant. In this context, taking a cue from materials made of uncross-linked linear polymer chains, one route might be to design a HCP network that undergoes some kind of structural rearrangement in the early stages of tensile deformation that hardens the material and thus makes the system brittle only after a large tensile deformation. This strain-dependent toughening of a material is known as "strain hardening" [1,2,16,17], which is known to play a key role in strengthening linear polymers against tensile deformation. In general, strain hardening in polymeric systems is associated with orientation of load-bearing covalent bonds in the direction of tensile deformation [1]. However, there is *a priori* no allowance for such a mechanism in HCPs. Therefore we investigate by means of extensive computer simulation if a HCP network can display strain hardening, and if so, what molecular-scale mechanisms give rise to this behavior.

We have performed coarse-grained molecular dynamics (MD) simulations to study a HCP model consisting of four-functional monomers confined between two impenetrable solid surfaces, one of which is fixed and the other allowed to move. In this model, individual monomers of the system interact with each other via a Lennard-Jones (LJ) potential [6,18]. Results are presented in terms of LJ energy u_o, LJ length d, and mass of the individual monomer m. This gives a characteristic time $\tau=\sqrt{md^2/u_o}$. Values representative of hydrocarbons are as follows: $u_o=30$ meV, $d=0.5$ nm, and $\tau=3$ ps. The unit of pressure is $p_o=40$ MPa [19]. For the interaction between bonded monomers we use the combination of a purely repulsive LJ potential and a quartic potential $V_{\mathrm{bond}}(r)=\kappa_4(y-r_1)(y-r_2)y^2+U_0$ for $r<1.5d$, while $V_{\mathrm{bond}}(r)=U_0$ for $r>1.5d$ [6]. Here $\kappa_4=1434.3u_o/d^4$, $y=r-\Delta r$, $\Delta r=1.5d$, $r_1=-0.7411d$, $r_2=0$, and $U_0=67.2234u_o$. Temperature is controlled by coupling the system to a Langevin thermostat with damping constant $\gamma=1/\tau$ and the equation of motion is integrated with a time step of $t_o=0.005\tau$.

Each confining wall consists of two layers of close-packed crystalline surfaces. The nearest-neighbor atomic spacing in a crystalline surface is $1.209d$. Initial configurations are generated by randomly distributing N monomers within the simulation box, which has linear dimensions L_x, L_y, and L_z in x, y, and z directions, respectively. Interaction between a monomer and a surface atom is the same as that of between two monomers. The system is then subjected to a 4000 MD time step warmup stage to remove the bead-bead overlaps using force capping. Once the fluid sample with excluded volume is successfully generated, the next step is to form a three-dimensional network. Based on the model po-

*debashish.mukherji@drexel.edu

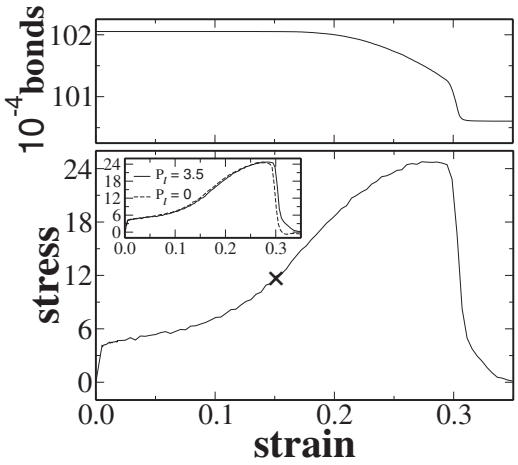

FIG. 1. Engineering stress as a function of engineering strain for a network with random bonding for a system size $N=510\,000$. Simulation was carried out at a constant strain rate $\dot{\epsilon}=2\times10^{-4}\tau^{-1}$ and thermal energy is set to 0.3 u_o/k_B. Symbol ($\times$) represents the strain value at which the first bond breaks. Top panel shows a plot of number of bonds as a function of strain. Inset shows a comparative plot obtained with and without pressure employed on the top surface.

tentials described above, bonds are allowed to form if the distance between monomers and between monomer and surface atoms is less than $1.3d$. During this curing stage the thermal energy is set to $1.1u_0/k_B$ and a constant compressive pressure, $P_l=3.5u_o/d^3$, is maintained on the top wall [20]. Each monomer is allowed to form at most four bonds with neighboring monomers and with surface atoms. Once 95% of all possible $4N/2$ bonds are formed, the system is quenched down to a temperature $0.3u_0/k_B$ also under a compressive pressure, P_l, and hence forms a dense highly cross-linked polymer glass. Tensile deformation is induced by pulling the upper wall with a velocity $\dot{L}_z$, giving an effective strain rate $\dot{\epsilon}=\dot{L}_z/L_z^o$, where L_z^o is the initial interwall separation. We have performed simulations at three different strain rates, i.e., $\dot{\epsilon}=10^{-3}\tau^{-1}$, $\dot{\epsilon}=5\times10^{-4}\tau^{-1}$, and $\dot{\epsilon}=2\times10^{-4}\tau^{-1}$. These rates are higher than typical experimental values. However, within the range of $\dot{\epsilon}$'s studied here we only observe a weak rate dependence. For our simulations, we have considered a system size of $N=510\,000$ within a box of linear dimensions of $L_x=L_y\approx85d$ and $L_z^o\approx76d$. All simulations are carried out three times with stochastically independent initial conditions. Results from individual runs differ from each other by a factor of less than 1%.

We plot engineering stress, σ, as a function of engineering strain, $\epsilon=(L_z-L_z^o)/L_z^o$, in Fig. 1 for a glassy state HCP network. We divide this plot into four distinct regimes: an initial regime, i.e., $\epsilon\leqslant1\%$ stress increases rapidly with a small network deformation. Above these strains (i.e., $1\%<\epsilon<15\%$), stress increases nonlinearly with increasing strain without breaking any bonds, as shown in the top panel of Fig. 1. Such behavior can be interpreted as the process during which the system becomes harder due to the external deformation, and thus is reminiscent of strain hardening in polymer glasses [2]. Beyond these strain values (i.e., $\epsilon>15\%$) an irreversible plastic deformation occurs and the first bond

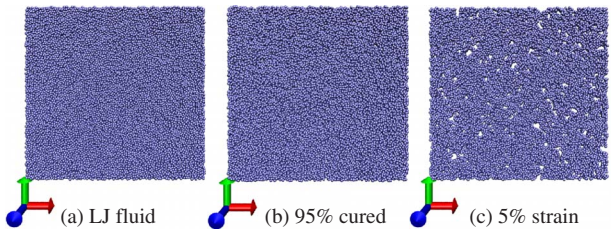

FIG. 2. (Color online) Simulation snapshots of a $85d\times85d\times2d$ slab for (a) LJ fluid at $\rho=0.93d^{-3}$, (b) 95% cured sample at $\rho=0.94d^{-3}$, and (c) after 5% strain at $\rho=0.87d^{-3}$. Here ρ is density of particle packings.

breaks at around $\epsilon\approx15\%$. Finally cohesive fracture occurs at $\epsilon\simeq30\%$. The inset in Fig. 1 contains a comparative plot, which indicates that within our parameter range stress-strain behavior is independent of whether or not any pressure is employed [20].

Stain hardening is a well-known phenomenon in thermoplastic materials [2], where the work done by tensile deformation is partially dissipated and partially stored in conformational changes of chains and often creation of internal surface area, in which case the phenomenon is typically referred to as crazing [21]. We find that strain hardening in our model HCP can also be explained due to the formation of microvoids that are uniformly distributed throughout the sample; see Fig. 2. One might guess whenever a surface is created, it is associated with broken bonds. However, no bonds break in the initial stages (i.e., during strain hardening) of void formation and growth.

Spontaneous void creation is known in dense LJ particle packings [22], where it is shown that density, $\rho=N/V$ with $V=(L_x\times L_y\times L_z)$, is the key factor in determining whether voids form. A "large" void can only form when ρ is smaller than a so-called critical density, ρ^*, and thus voids grow in size with the reduction in ρ. In our simulations, ρ decreases with increasing tensile deformation, consistent with increasing void size with increasing ϵ. It is important to mention that brittle fracture will occur if there was one dominant large void in the sample. Moreover, strain hardening is only made possible because of the presence of many small voids as shown in part (c) of Fig. 2. Therefore it is important to understand what determines the distribution of void sizes. For this purpose, we discretize our simulation domain into V/v_{voxel} cubic voxels, each with volume v_{voxel}. In a series of simulations, the voxel size is varied from $0.1d^3<v_{\text{voxel}}<0.5d^3$, depending on the temperature at which void distribution is observed. A box is considered to be void space if there is no monomer inside it and also the centroid of a monomer is farther than $d/2$ distance from the box boundary. Empty boxes are clustered into voids according to the rule that any two empty face-sharing voxels must belong to the same void. Subsequently, void size is measured as the number of voxels in a distinct void times the volume of a single voxel.

We show the distribution function, $P(v)$, in Fig. 3. $P(v)$ appears to obey one universal master curve, independent of strain (so long as no bonds are broken). We observe that the data are easily described by a distribution function well-known from LJ particle packings [23,24],

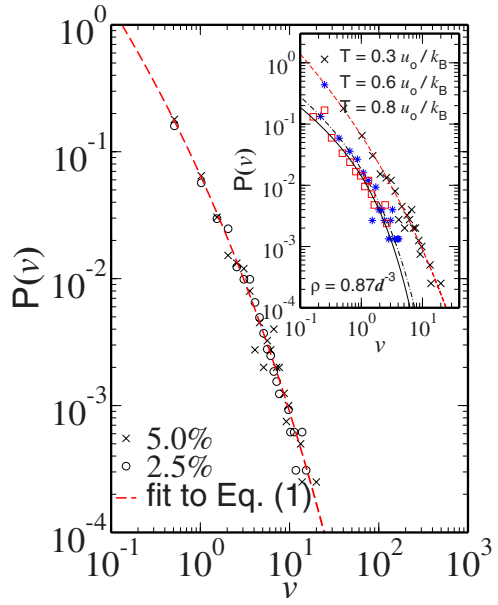

FIG. 3. (Color online) Void size distribution at two different strains, ϵ, that corresponds to densities $\rho=0.91d^{-3}$ for $\epsilon=2.5\%$ and $\rho=0.87d^{-3}$ for $\epsilon=5\%$, respectively. Here $P(v)$ is the normalized distribution function $n(v)/\Sigma_v n(v)$ and $n(v)$ is the number of voids with volume v. Dashed curve is a fit according to Eq. (1) with $\alpha=0.32$ and $\zeta=0.27$. Inset shows the distribution function $P(v)$ at three different temperatures at a density $\rho=0.87d^{-3}$. The curves are fits with (α,ζ) to be (0.32,0.27) for $T=0.3u_o/k_B$, (0.36,0.60) for $T=0.6u_o/k_B$, and (0.32,0.75) for $T=0.8u_o/k_B$, respectively. All simulations are carried out at $\dot{\epsilon}=2\times10^{-4}\tau^{-1}$.

$$P(v)=\frac{n(v)}{\Sigma_v n(v)}\propto v^{\alpha-1}\exp\left(-\frac{E_p}{k_B T}\right), \tag{1}$$

where $n(v)$ is the number of voids with volume v and E_p is size dependent pseudoenergy that scales as v^{ζ}. Here α and ζ are positive fitting parameters. Fitting Eq. (1) to the data in Fig. 3, we find $\alpha=0.32$ and $\zeta=0.27$. A comparison of void sizes in the HCP to those of the LJ fluid suggests that individual void sizes in the HCP are two orders of magnitude larger, yet their distribution can be described by the same empirical function. Smaller voids in the LJ particle packings are predominantly interstitial, which grow in size with reduction in ρ [24]. In our HCP network we observe a similar trend from the unnormalized data of void size, $n(v)$, that shows two distinct features: with increasing strain, the number of voids corresponding to a particular size increases. The second trend is that, at larger strains, we observe large voids that are absent at smaller strains.

Despite the long history of the statistical thermodynamics of void space in dense particle packings [23–25], there remains as yet no clear interpretation of the physical meaning of the form and parameter values of Eq. (1). It is yet interesting that the relatively large voids, as we observe in our HCP, also obey the same functional dependence. Here we speculate a possible origin for the two different contributions as in Eq. (1). From Fig. 3 it is clear that the void volume is distributed such that smaller voids are more numerous so that the surface area can be distributed over as many voids as possible. Furthermore, Eq. (1) states that the distribution of void volume has two main influences: the first factor, $v^{-2/3}$, corresponds to the surface energy, while the second factor is Boltzmann-like, which measures the energetic penalty for the creation of a void of size v from a homogeneous chunk of material at a given ρ. We find this pseudoenergy, E_p, scales as $v^{0.27}$ for a HCP sample in its glassy state. To further analyze the effect of temperature in our system, we have also performed void analysis at two other temperatures, $0.6u_o/k_B$ and $0.8u_o/k_B$, as shown in the inset of Fig. 3. Data for different temperatures are again well fit by Eq. (1) with varying only the exponent ζ and the exponent α remains the same within the stochastic error bar, which suggests that E_p is somehow temperature dependent. It can be seen from the comparative plot in the inset of Fig. 3 that the probability of finding large voids is extremely unlikely at large temperatures. This is somewhat surprising, given that one would expect to see a long tail in the distribution function at large temperatures. This contradiction can be understood in terms of critical density, ρ^*, which decreases with increasing temperature and thus is consistent with the absence of larger voids, for $T>0.3u_o/k_B$.

We also investigated void shapes using their gyration tensors. Large voids were predominantly pancake-shaped with the small axis oriented in the direction of tensile deformation. Furthermore, the lateral dimensions of the largest void of size $v\approx25d^3$ prior to any bond breaking is $6d$, which is much larger than the maximum extension of the intermonomer bonds (i.e., $1.5d$). Existence of such large voids can only be explained by the intermonomer bond orientation. Within a simple probabilistic argument of forming four bonds, by a particle, out of its 12 nearest neighbor in a precured LJ sample, we would argue that these protovoid nucleation sites are already encoded into the system during its curing process. Indeed, by analyzing the bond orientation in the simulation snapshots, it is apparent that almost 95% of the monomers in the periphery of such voids are four-coordinated. However, most of the bonds emanating from these peripheral particles are oriented away from the void center. Thus increasing void size with ϵ is due to the disruption of contacts between nonbonded monomers. This explains why we observe voids without bond breaking. This particular surface drawing is analogous to crazing in glassy thermoplastic polymers [21], which usually occurs in regions of high localized tension and results in toughening. Moreover, upon increasing strain above 15%, these microcracks propagate in the lateral direction due to bond breaking near their periphery, leading ultimately to fracture in the sample.

It is yet important to point out that the specific spatial distribution of the monomers is only made possible because bonds are allowed arbitrary orientation, so long as particles do not overlap. Therefore, by imposing an additional bond angle constraint, giving a particular geometry to the system, the so-called strain hardening behavior should disappear. We therefore assessed the effect of imposing tetrahedral arrangements by using an additional bonding potential $V_{\text{angle}}(\theta_{ijk})=\kappa_\theta(\theta_{ijk}-\theta_0)^2$, where $\theta_0=109.45°$, $\kappa_\theta=0.02$, and θ_{ijk} is the angle between bond vectors b_{ij} and b_{jk}. We have conducted a series of simulations where κ_θ is varied from 0.001 to 0.02 and strain hardening is not observed when $\kappa_\theta>0.005$. Simi-

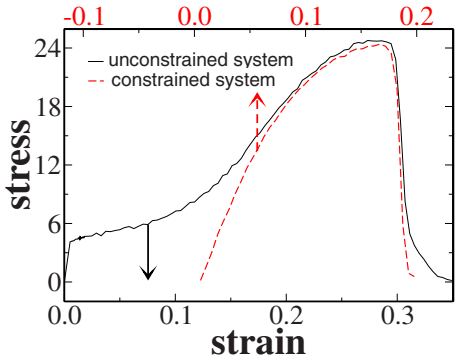

FIG. 4. (Color online) Comparison of stress-strain plot for an unconstrained (solid) and a bond-angle-constrained (dashed shifted) system. Simulations are carried out at a constant strain rate $\dot{\epsilon}=2\times10^{-4}\tau^{-1}$ and thermal energy $0.3u_o/k_B$. Arrows indicate the x axis of a particular curve.

lar to that of an unconstrained system, here also we achieve a 95% cure. A stress-strain curve for a constrained system is compared to that of an unconstrained system in Fig. 4. The constrained system does not show strain hardening behavior and first bond break at around 2% strain [20]. However, it is interesting to note that the two models display nearly identical stress-strain behavior in the posthardened phase. As anticipated, we observe no voids in the constrained system. Thus we conclude that bond angle rearrangement makes a HCP tougher by engaging a microvoid based strain hardening mechanism and hence less ductile.

In conclusion, we have performed MD simulations to study the mechanical behavior of HCPs. We investigated two geometrically distinct model HCPs. In one case intermonomer bonding can have any arbitrary arrangement (unconstrained system) and in another case we impose tetrahedral bonding (constrained system). In the former case we observe a strain hardening behavior due to creation and growth of microvoids. The void size distribution obeys a function well known from LJ particle packings [24]. Microvoid formation was made possible due to the random orientation of bonds. Strain hardening makes the unconstrained network ductile. In the latter case, the bond angle constraints prevented microvoid formation and strain hardening. Therefore we suggest that a possible route toward designing ductility into the HCP network might involve flexible cross-linkers.

Financial support from the U.S. Army Research Lab through Grants No. W911NF-06-2-0013 and No. W911NF-07-1-0301 and the ACS Petroleum Research Fund (42368-G7) is gratefully acknowledged.

[1] L. R. G. Treloar, *The Physics of Rubber Elasticity* (Clarendon, Oxford, 1975).
[2] *The Physics of Glassy Polymers*, edited by R. N. Haward and R. J. Young (Chapman and Hall, London, 1997).
[3] A. Baljon and M. O. Robbins, Science **271**, 482 (1996).
[4] T. Hölzl, H. L. Trautenberg, and D. Göritz, Phys. Rev. Lett. **79**, 2293 (1997).
[5] S. W. Sides, G. S. Grest, and M. J. Stevens, Phys. Rev. E **64**, 050802(R) (2001).
[6] M. J. Stevens, Macromolecules **34**, 2710 (2001).
[7] X. Chen, F. Wudl, A. K. Mal, H. Shen, and S. R. Nutt, Macromolecules **36**, 1802 (2003).
[8] M. Tsige and M. J. Stevens, Macromolecules **37**, 630 (2004); M. Tsige, C. D. Lorenz, and M. J. Stevens, *ibid.* **37**, 8466 (2004).
[9] S. R. White, N. R. Sottos, P. H. Geubelle, J. S. Moore, M. R. Kessler, S. R. Sriram, E. N. Brown, and S. Viswanathan, Nature (London) **409**, 794 (2001).
[10] X. Chen, M. A. Dam, K. Ono, A. Mal, H. B. Shen, S. R. Nutt, K. Sheran, and F. Wudl, Science **295**, 1698 (2002).
[11] K. S. Toohey, N. R. Sottos, J. A. Lewis, J. S. Moore, and S. R. White, Nature Mater. **6**, 581 (2007).
[12] G. de Crevoisier, P. Fabre, and J. C. L. Leibler, Science **285**, 1246 (1999).
[13] M. J. Stevens, Macromolecules **34**, 1411 (2001).
[14] P. V. Komarov, C. Yu-Tsung, C. Shih-Ming, P. G. Khalatur, and P. Reineker, Macromolecules **40**, 8104 (2007).
[15] J. Jang, C. K. Ullal, T. Choi, M. C. Lemieux, V. V. Tsukruk, and E. L. Thomas, Adv. Mater. (Weinheim, Ger.) **18**, 2123 (2006).
[16] K. J. Calzia, A. Forcum, and A. J. Lesser, J. Appl. Polym. Sci. **102**, 4606 (2006).
[17] R. S. Hoy and M. O. Robbins, Phys. Rev. Lett. **99**, 117801 (2007).
[18] K. Kremer and G. S. Grest, J. Chem. Phys. **92**, 5057 (1990).
[19] D. Mukherji and M. H. Müser, Macromolecules **40**, 1754 (2007).
[20] See EPAPS Document No. E-PLEEE8-78-R03811 for auxiliary documentation. For more information on EPAPS, see http://www.aip.org/pubservs/epaps.html.
[21] J. Rottler, S. Barsky, and M. O. Robbins, Phys. Rev. Lett. **89**, 148304 (2002).
[22] S. Sastry, P. G. Debenedetti, and F. H. Stillinger, Phys. Rev. E **56**, 5533 (1997).
[23] W. G. Hoover, N. E. Hoover, and K. Hanson, J. Chem. Phys. **70**, 1837 (1979).
[24] S. Sastry, T. M. Truskett, P. G. Debenedetti, S. Torquato, and F. H. Stillinger, Mol. Phys. **95**, 289 (1998).
[25] J. L. Meijering, Philips Res. Rep. **8**, 270 (1953); R. J. Speedy and H. Reiss, Mol. Phys. **72**, 999 (1991).